

Anisotropic Friedel oscillations in graphene-like materials: The Dirac point approximation in wave-number dependent quantities revisited

T. Farajollahpour, S. Khamouei, S. Safari Shateri and A. Phirouznia^{1,*}

¹*Department of Physics, Azarbaijan Shahid Madani University, 53714-161, Tabriz, Iran*
Condensed Matter Computational Research Lab. Azarbaijan Shahid Madani University, 53714-161, Tabriz, Iran
 (Dated: January 25, 2016)

Friedel oscillations of the graphene-like materials are investigated theoretically beyond the Dirac point-approximation. Numerical calculations have been performed within the random phase approximation (RPA). For intra-valley transitions it was demonstrated that the contribution of the different Dirac points in the wave-number dependent quantities, such as dielectric function $\epsilon(\vec{q})$, has been determined by the orientation of the wave-number with respect to the Dirac point position vector in k -space. Therefore identical contribution of the different Dirac points is not automatically guaranteed by the degeneracy of the Hamiltonian at these points. Meanwhile it was shown that the contribution of the inter-valley transitions is always anisotropic even when the Dirac points coincide with the Fermi level ($E_F = 0$). This means that the Dirac point approximation based studies give the correct physics only at high wave length limit. The anisotropy of the static dielectric function reveals different contribution of the each Dirac point. Additionally, the anisotropic k -space dielectric function results in anisotropic Friedel oscillations in graphene-like materials. Calculations have also been performed in the presence of the Rashba interaction. It was shown that increasing the Rashba interaction strength slightly modifies the Friedel oscillations in graphene-like materials. Therefore the anisotropic dielectric function in k -space is the clear manifestation of band anisotropy in the graphene-like systems.

PACS numbers: 77.22.-d 71.45.Gm 73.22.-f

I. INTRODUCTION

At the present time monolayer structures are one of the most reach and fast growing fields of condensed matter physics. Experimental observation of graphene in 2004^{1,2} has created a great motivation in scientists to discovery and study of other possible two-dimensional (2D) allotropes of IV group elements in periodic table such as silicene, germanene and recently stanene³. These new 2D materials and other buckled honeycomb lattice structures predicted in theoretical works such as Ref. [4–7] and several experimental synthesization have also been performed for realization of these materials^{8–11}. The silicon and germanium analog of graphene with slightly buckled honeycomb geometry were predicted to have a Dirac cone and the electrons follow the massless Dirac equation near the Fermi level^{12–14}.

There are some distinctions between these new 2D materials and graphene. Unlike graphene, the hybridization of π bonds in silicene is not pure and the structure of silicene shows a mixed hybridization. The π electrons in silicene are much more active than graphene and this lead to a different structure from graphene¹⁵. Similar to the graphene structure, silicon atoms are arrayed in a hexagonal lattice, but with a slight buckling that proven by first principle studies which show low buckled silicene is thermally stable⁵. It was also shown that the electronic dispersion of the silicene near K points of the first Brillouin zone is linear similar to the behavior of Dirac materials^{4,5,16,17}. Since the flat configuration of silicene is not stable⁵ the buckled configuration of silicene is more interesting for research activities.

The spin orbit coupling (SOC) in silicene is more stronger than graphene, this leads to relatively large energy gap at the Dirac points (Δ_{SO}). Strong SOC in silicene makes this monolayer a good candidate for topological insulators and quantum spin Hall effect (QSHE)⁶. Another considerable phenomenon in the monolayer silicene is appeared when an external electric field is applied. By applying a normal electric field, E_z , an on-site potential difference of $\Delta_z = E_z l$ is created between sublattices where l is the separation of the sublattices¹⁸. The band gap in silicene (germanene) is tunable by an external electric field which is perpendicular to the silicene (germanene) sheet^{19,20}. In this case the value of E_z plays an important role so that for Δ_z is greater than Δ_{SO} , the system turns from a topological insulator to a band insulator^{20,21} and when $\Delta_z = \Delta_{SO}$, the system is a valley-spin polarized metal²². Bilayer graphene has also been studied in the present work. The bilayer graphene has an advantage in comparison with the monolayer graphene since an applied gate voltage changes the potential of each layer and opens a direct gap that converts the bilayer graphene from a semimetal to a semiconductor²³.

It has been generally assumed that the degeneracy of the Dirac points provides the identical contribution of these points in the physical quantities. This could be a correct procedure and would be valid for calculation of the scalar quantities. However, it should be noted that the Dirac points in k -space are not distributed isotropically. This anisotropy has been dictated by the band anisotropy of the honeycomb structures in the k -space. Therefore identical treatment of the Dirac points auto-

matically ignores anisotropy of the band energy. It seems that this anisotropy could be appeared just at high Fermi energies. However, as it was shown in this work, even in the case of $E_F = 0$ in which the Fermi level matches the Dirac points the contribution of inter-valley transitions are completely anisotropic.

Within the Dirac point approximation when the Dirac points have been treated identically, anisotropic effects have been completely ignored at low Fermi energies. Some of the anisotropic effects are raised by increasing the Fermi energy up to the range of trigonal warping effects. However, even at low Fermi energies band anisotropy of the system manifests itself in the dielectric function, $\epsilon(\vec{q})$, at least at the range of inter-valley transitions where $q \sim |\mathbf{K}_D - \mathbf{K}'_D|$ in which \mathbf{K}_D and \mathbf{K}'_D are different Dirac points. Since the band energy of the system has been reduced to a cone-like dispersion. In this case the Fermi level has been identified with a symmetric circle around the Dirac points known as Fermi circle. Hence, calculation of the wave number dependent quantities should be performed with some care since the direction of the transferred momentum, \vec{q} , determines the contribution of each Dirac point in both intra-valley and inter-valley transitions. for a given transferred momentum, \vec{q} , different Dirac points have not the same contribution in this type of the physical quantities. This work attempts to provide some insight into the limitations of identical treatment of the Dirac points. Results of the current work emphasize the need for a systematic revision of identical treatment validity of the Dirac points in different types of quantities. Specifically, we analyze the robustness of the band anisotropy in graphene and other honeycomb systems which manifests itself in the dielectric function and Friedel oscillations of the system. To this end, random phase approximation (RPA) is employed beyond the Dirac point approximation.

It should be noted that the band induced anisotropic effects could be obtained even when the Fermi energy is close to the Dirac points. This is due to the fact that the optical transitions which could be available for a given transferred momentum \vec{q} are not identical for different Dirac points in k -space. At the level of the Dirac point approximation anisotropic position of the Dirac points and its relevant effects have been ignored. However, the anisotropy of single Fermi circle reshaping, which arises by increasing the Fermi energy, could be obtained within this approach. In the present work we have obtained the anisotropic properties which could be originated from the anisotropic location of the Dirac points at low Fermi energies. It is obvious that nonlinear energy dispersion at high Fermi energies could effectively take into account beyond the Dirac point approximation. If we use the exact numerical approach and set aside the Dirac cone approximation even at low Fermi energies we could obtain the band induced anisotropy which was the main idea of the current study.

The unique optical and electronic properties of graphene-like systems such as silicene has made these

TABLE I: Lattice constant and Energy scales for graphene and other buckled honeycomb materials^{6,20,33,34}.

material	a	t	t_{SO}	t_{intR}
silicene	3.86 Å	1.6 eV	0.75 meV	0.46 meV
germanene	4.02 Å	1.3 eV	8.27 meV	7.13 meV
graphene	2.46 Å	2.8 eV	0.00114 meV	—

materials a good candidate for plasmonics applications. Meanwhile plasmonic-based studies has already been performed for graphene however, the other graphene-like systems are known as highly appealing subjects for this field of condensed matter physics^{24–27}.

Friedel oscillation has been reported for graphene in low energy Hamiltonian which relies on the Dirac-cone approximation^{28–31}. These approaches ignore the contribution comes from the nonlinear part of the spectrum however this can be reasonable when the Fermi energy is close to the Dirac points. Nevertheless, as mentioned before the Dirac point approximation cannot capture the anisotropic contribution of each Dirac points in wave-number dependent quantities. It should be noted, the anisotropic contributions are not limited to the contribution of non-linear bands of high energy states. At low Fermi energies there is also another type of anisotropic behaviors in wave number dependent quantities originate from non-identical contribution of the Dirac points. In this work calculations have been performed beyond the Dirac point approximation in which all possible types of the band anisotropy, including the nonlinear part of the spectrum, have been considered. Meanwhile, it should be noted that the linear dispersion at Dirac points in silicene is being seriously debated³². Motivated by the mentioned points about the identical treatment of the Dirac points we have performed current numerical study to obtain a better understanding about the limitations of the Dirac point approximation in graphene-like systems.

This paper is organized as follows. In Sec. II the Hamiltonian of the honeycomb systems in the presence of extrinsic Rashba term is introduced. In Sec. III the random phase approximation is briefly discussed and numerical result for dielectric function are presented. Sec. IV is devoted to the analysis of charge impurity in the presence of extrinsic Rashba coupling. Sec. V presents our results and finally we conclude this paper in Sec. VI.

II. TIGHT-BINDING HAMILTONIAN OF GRAPHENE LIKE STRUCTURES

A. graphene, silicene and germanene

The crystal structure of graphene-like materials is a honeycomb lattice, similar to graphene, the SOC for buckled honeycomb has two component, one is parallel

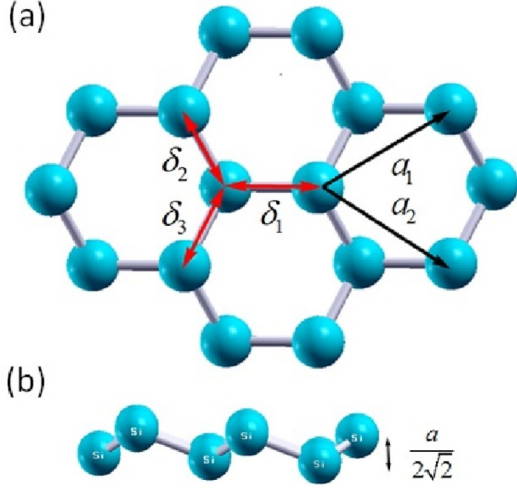


FIG. 1: (Color online) (a) hexagonal structure of buckled two dimensional lattice where $\delta_1 = a(1, 0, 1/2\sqrt{2})$, $\delta_2 = a(-1/2, \sqrt{3}/2, 1/2\sqrt{2})$, $\delta_3 = a(-1/2, -\sqrt{3}/2, 1/2\sqrt{2})$ are the next nearest neighbors position vectors, the lattice vectors are $\mathbf{a}_1 = \frac{a}{2}(3, \sqrt{3})$, $\mathbf{a}_2 = \frac{a}{2}(3, -\sqrt{3})$, and the next nearest position vectors are $\delta'_1 = \pm\mathbf{a}_1$, $\delta'_2 = \pm\mathbf{a}_2$ and $\delta'_3 = \pm(\mathbf{a}_2 - \mathbf{a}_1)$. (b) Side view of buckled structure for silicene.

to the plane and other is perpendicular.

The Hamiltonian of the buckled honeycomb lattice in tight-binding approximation in the presence of SOC's can be written as

$$\begin{aligned}
 H = & -t \sum_{\langle ij \rangle \alpha} \hat{c}_{i\alpha}^\dagger \hat{c}_{j\alpha} + it_{SO} \sum_{\langle\langle ij \rangle\rangle \alpha\beta} v_{ij} \hat{c}_{i\alpha}^\dagger \sigma_{\alpha\beta}^z \hat{c}_{j\beta} \\
 & - it_{intR} \sum_{\langle\langle ij \rangle\rangle \alpha\beta} \mu_{ij} \hat{c}_{i\alpha}^\dagger (\vec{\sigma} \times \vec{d}_{ij})_{\alpha\beta}^z \hat{c}_{j\beta} \\
 & + it_{extR} \sum_{\langle ij \rangle \alpha\beta} \hat{c}_{i\alpha}^\dagger (\vec{\sigma} \times \vec{d}_{ij})_{\alpha\beta}^z \hat{c}_{j\beta}. \quad (2.1)
 \end{aligned}$$

A new type of the SOC arises due to intrinsic buckled geometry of silicene and germanene. In the tight-binding approximation of these graphene-like structures intrinsic buckled configuration results in intrinsic Rashba type interaction^{12,20,22,33}. Hamiltonian of the germanene, which is also a honeycomb structure of group IV elements, is similar to that of the silicene and the difference is just due to the various parameter values that were listed in table I. The individual terms of the Hamiltonian could be described as follows: The first term of this noninteracting Hamiltonian is the nearest neighbor hopping contribution given by

$$H_0 = -t \sum_{\langle ij \rangle \alpha} \hat{c}_{i\alpha}^\dagger \hat{c}_{j\alpha}, \quad (2.2)$$

Where the sum is taken over all pairs of the nearest-neighboring sites, and the operator $\hat{c}_{j\alpha}^\dagger$ ($\hat{c}_{j\alpha}$) creates (annihilates) an electron with spin α at site j and t is the

nearest neighbor hopping amplitude. The values of these parameters for different materials are given in table I. By performing a Fourier transformation, the first term of the Hamiltonian on the basis of $\{\Psi_{A\uparrow}, \Psi_{A\downarrow}, \Psi_{B\uparrow}, \Psi_{B\downarrow}\}$ reads

$$H_0 = -t \int d^2k \hat{\Psi}^\dagger(k) M_{4 \times 4}^0 \hat{\Psi}(k), \quad (2.3)$$

where

$$M_{4 \times 4}^0 = \begin{pmatrix} 0 & 0 & \gamma_k & 0 \\ 0 & 0 & 0 & \gamma_k \\ \gamma_k^* & 0 & 0 & 0 \\ 0 & \gamma_k^* & 0 & 0 \end{pmatrix} \quad (2.4)$$

and $|\gamma|^2 = 1 + 4 \cos(\sqrt{3}/2 ak_y) \cos(3/2 ak_x) + 4 \cos^2(\sqrt{3}/2 ak_y)$. The next term of the Hamiltonian describes the spin-orbit interaction and one has to distinguish between the parallel (with the plane) and perpendicular components of the SOC. The parallel term is as follows

$$H_{SO} = it_{SO} \sum_{\langle\langle ij \rangle\rangle \alpha\beta} u_{ij} \hat{c}_{i\alpha}^\dagger \sigma_{\alpha\beta}^z \hat{c}_{j\beta}, \quad (2.5)$$

where t_{SO} is the next-nearest neighbor hopping, $u_{ij} = \frac{\vec{d}_i \times \vec{d}_j}{|\vec{d}_i \times \vec{d}_j|}$ where \vec{d}_i and \vec{d}_j are the two nearest bonds that connect the next-nearest neighbors. Where $u_{ij} = 1$ if the next-nearest neighbor hopping is counterclockwise and $u_{ij} = -1$ when it is clockwise with respect to the positive z axis¹⁸. The $\langle\langle ij \rangle\rangle$ run over all the next-nearest neighbor hopping sites and σ_z is the Pauli matrix. Performing the Fourier transformation on H_{SO} yields

$$H_{SO} = t_{SO} \int d^2k \hat{\Psi}^\dagger(k) M_{4 \times 4}^{SO} \hat{\Psi}(k), \quad (2.6)$$

where

$$M_{4 \times 4}^{SO} = \begin{pmatrix} \eta & 0 & 0 & 0 \\ 0 & -\eta & 0 & 0 \\ 0 & 0 & -\eta & 0 \\ 0 & 0 & 0 & \eta \end{pmatrix} \quad (2.7)$$

and

$$\eta = 2 \sin(k_y a) - 4 \sin\left(\frac{\sqrt{3}}{2} k_x a\right) \cos\left(\frac{k_y a}{2}\right). \quad (2.8)$$

The perpendicular term or intrinsic Rashba SOC is given by

$$H_{intR} = -it_{intR} \sum_{\langle\langle ij \rangle\rangle \alpha\beta} \mu_{ij} \hat{c}_{i\alpha}^\dagger (\vec{\sigma} \times \vec{d}_{ij})_{\alpha\beta}^z \hat{c}_{j\beta}, \quad (2.9)$$

where t_{intR} is the strength of intrinsic Rashba SOC and $\mu_{ij} = \pm 1$ for the A (B) site. We can rewrite this term as

$$H_{intR} = -t_{intR} \int d^2k \hat{\Psi}^\dagger(k) M_{4 \times 4}^{intR} \hat{\Psi}(k), \quad (2.10)$$

in which

$$M_{4 \times 4}^{\text{int } R} = \begin{pmatrix} 0 & 0 & 0 & i\lambda_+ \\ 0 & 0 & i\lambda_- & 0 \\ 0 & -i\lambda_-^* & 0 & 0 \\ -i\lambda_+^* & 0 & 0 & 0 \end{pmatrix}, \quad (2.11)$$

where $\lambda_+ = \lambda_1 + \lambda_2$ and $\lambda_- = \lambda_1 - \lambda_2$,

$$\lambda_1 = 2i \left[\sin(k_y a) - \sin\left(\frac{k_y a}{2}\right) \cos\left(\frac{\sqrt{3}}{2} k_x a\right) \right] \quad (2.12)$$

$$\lambda_2 = \left[2\sqrt{3} \cos\left(\frac{k_y a}{2}\right) \cos\left(\frac{\sqrt{3}}{2} k_x a\right) \right]. \quad (2.13)$$

The last term is the external Rashba interaction

$$H_{\text{ext } R} = i t_{\text{ext } R} \sum_{\langle ij \rangle \alpha \beta} \hat{c}_{i\alpha}^\dagger \left(\vec{\sigma} \times \vec{d}_{ij} \right)_{\alpha\beta}^z \hat{c}_{j\beta} \quad (2.14)$$

The strength of the external Rashba coupling can be manipulated by an external gate voltage or by the substrate. The extrinsic Rashba coupling arises as a result of the inversion symmetry breaking due to an applied perpendicular electric field or interaction with substrate³⁵. Similarly this term can be written as

$$H_{\text{ext } R} = t_{\text{ext } R} \int d^2 k \hat{\Psi}^\dagger(k) M_{4 \times 4}^{\text{ext } R} \hat{\Psi}(k), \quad (2.15)$$

where we have defined

$$M_{4 \times 4}^{\text{ext } R} = \begin{pmatrix} 0 & 0 & 0 & i\beta_+ \\ 0 & 0 & i\beta_- & 0 \\ 0 & -i\beta_-^* & 0 & 0 \\ -i\beta_+^* & 0 & 0 & 0 \end{pmatrix}, \quad (2.16)$$

and $\beta_+ = \beta_1 + \beta_2$ and $\beta_- = \beta_1 - \beta_2$,

$$\beta_1 = \exp\left(-i \frac{ak_x}{2\sqrt{3}}\right) \sin\left(\frac{ak_y}{2}\right) \quad (2.17)$$

$$\beta_2 = \frac{\sqrt{3}}{3} \left(\exp\left(i \frac{ak_x}{\sqrt{3}}\right) + \exp\left(-i \frac{ak_x}{\sqrt{3}}\right) \cos\left(\frac{ak_y}{2}\right) \right). \quad (2.18)$$

We have obtained the Hamiltonian throughout the Brillouin zone of buckled honeycomb lattice such as silicene and germanene and also for graphene monolayer. It should be noted that the intrinsic Rashba interaction vanishes for graphene. This is due to the fact that the monolayer graphene has been assumed buckling free. Similarly in the next section we focus on the bilayer graphene tight-binding Hamiltonian.

B. Bilayer graphene

The Hamiltonian of the multi-layer graphene structures depends on stacking of the layers^{36,37}. In this work

since the Bernal stacking is more common than the other configurations, for example AA stacking, calculations has been performed for Bernal stacking in which the two layers of graphene are in the form that one of the layers rotated by 60 degree with respect other one³⁷. The generalization of monolayer graphene Hamiltonian to bilayer system is straightforward. The noninteracting Hamiltonian in the basis:

$$\Psi(k) = \left\{ \Psi_{A\uparrow}^1, \Psi_{A\downarrow}^1, \Psi_{B\uparrow}^1, \Psi_{B\downarrow}^1, \Psi_{A\uparrow}^2, \Psi_{A\downarrow}^2, \Psi_{B\uparrow}^2, \Psi_{B\downarrow}^2 \right\},$$

is

$$H_0^{BLG} = \int d^2 k \Psi^\dagger(k) M_{8 \times 8}^0 \Psi(k), \quad (2.19)$$

where the indices 1 and 2 are labels for the layers of graphene. The matrix representation of $M_{8 \times 8}^0$ is as follows

$$M_{8 \times 8}^0 = \begin{pmatrix} t M_{4 \times 4}^0 & A \\ A^\dagger & t M_{4 \times 4}^0 \end{pmatrix} \quad (2.20)$$

$$A = \begin{pmatrix} 0 & 0 & t_\perp & 0 \\ 0 & 0 & 0 & t_\perp \\ 0 & 0 & 0 & 0 \\ 0 & 0 & 0 & 0 \end{pmatrix},$$

t_\perp is an inter-layer hopping parameter and is in the order of $(0.1 - 0.2)t$. The presence of spin orbit interaction simply opens a band gap in the spectrum of the bilayer graphene³⁸. The spin orbit interaction term of bilayer graphene is given by,

$$H_{SO}^{BLG} = t_{SO} \int d^2 k \Psi^\dagger(k) M_{8 \times 8}^{SO} \Psi(k) \quad (2.21)$$

$$M_{8 \times 8}^{SO} = \begin{pmatrix} M_{4 \times 4}^{SO} & 0 \\ 0 & M_{4 \times 4}^{SO} \end{pmatrix}, \quad (2.22)$$

the H_R^{BLG} describes the external Rashba spin orbit interaction with coupling strength $t_{\text{ext } R}$, the regarded Rashba term gives an expectation that a perpendicular electric field creates intra-layer Rashba term in the same way for a monolayer graphene.

$$H_R^{BLG} = t_{\text{ext } R} \int d^2 k \Psi^\dagger(k) M_{8 \times 8}^R \Psi(k), \quad (2.23)$$

$$M_{8 \times 8}^R = \begin{pmatrix} M_{4 \times 4}^R & 0 \\ 0 & M_{4 \times 4}^R \end{pmatrix}, \quad (2.24)$$

We have assumed that the Rashba SOC strength in the top and bottom graphene layers of bilayer graphene are equal. The unequal value of Rashba coupling strength in bilayer graphene systems show an topological phase transition which occur in a critical value of Rashba strength³⁹. In the next section the polarization function and Friedel oscillation in these systems in the presence of different value of extrinsic Rashba term will be investigated.

III. POLARIZATION FUNCTION

Dielectric function and the screening of the charged impurity and also the dynamical polarization which gives collective excitations could be captured by the polarization function $\Pi(\omega, q)$. Dielectric function and collective density oscillations of an electron liquid, are known as plasmons, have been observed in different metals and superconductors^{40,41}. At the static limit ($\hbar\omega = 0$) polarization function gives the screening behavior of the coulomb potential. The dielectric function is relevant to plasmonic studies meanwhile the transport and phonon spectra are also another relevant fields⁴².

In the current study we have focused on the tight-binding approximation of graphene-like structures. The electron-electron interaction has been considered within the random phase approximation characterizes by the density-density correlation function or polarization function^{28,29,41,43–49}. In this approach dielectric function is given by

$$\epsilon(\omega, q) = 1 - V(q) \Pi(\omega, q) \quad (3.1)$$

Where $V(q)$ is the 2D Coulomb potential, here $V(q) = 2\pi e^2/q$. Within the Dirac point approximation an effective Coulomb potential could be employed in which $V(q) = 2\pi\alpha/q$ and α is the ratio of coulomb to kinetic energy and named effective fine structure constant where equal to $\alpha = e^2/(\hbar\varepsilon_0 v)$ and ε_0 is the bare dielectric constant. Unlike to the graphene where the value of fine structure constant could be determined experimentally for different substrates⁵⁰, one can set $\alpha = 0.8^{26}$ for other buckled honeycomb lattices. The polarization function in one loop approximation is calculated directly from the bubble diagram that shown in Fig (2).

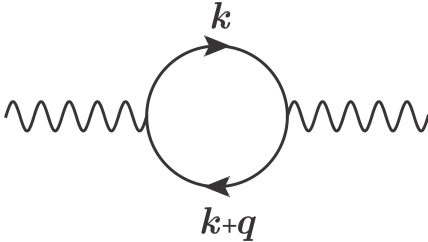


FIG. 2: The bare polarization bubble diagram corresponding to Eq. (3.2).

$$\begin{aligned} \Pi(q, \omega) &= \sum_{ss'kk'} \frac{f_k^s - f_{k+q}^{s'}}{\omega + E_k^s - E_{k+q}^{s'}} F_{s's'}(k', k) \\ &= \sum_{ss'k} \frac{f_k^s - f_{k+q}^{s'}}{\omega + E_k^s - E_{k+q}^{s'}} F_{s's'}(k + q, k), \end{aligned} \quad (3.2)$$

here, the summation performed over the full Brillouin zone and all of the spin and pseudo-spin dependent eigenstates in which $f_k^s = \frac{1}{\exp \beta(E_k^s - E_F) + 1}$ is the Fermi distribution function, and E_F is the Fermi energy. The form

factor is given by $F_{s's}(\vec{k}', \vec{k}) = \langle k' \lambda_{k'}^{s'} | e^{iq \cdot r} | k \lambda_k^s \rangle = \langle k' \lambda_{k'}^{s'} | k \lambda_k^s \rangle \delta_{\vec{k}', \vec{k} + \vec{q}}$ in which $|k \lambda_k^s\rangle = |k\rangle \otimes |\lambda_k^s\rangle$ are the eigenstates of the Hamiltonian where $|\lambda_k^s\rangle$ is the eigenstate in the spin and pseudo-spin subspaces. $\delta_{\vec{k}', \vec{k} + \vec{q}}$ represents the momentum conservation rule as a general condition for contributing transitions.

Within the Dirac point approximation the above expression of the polarization function has been assumed to be²⁹

$$\Pi(q, \omega) = g \sum_{ss'k} \frac{f_k^s - f_{k+q}^{s'}}{\omega + E_k^s - E_{k+q}^{s'}} F_{s's'}(\vec{k} + \vec{q}, \vec{k}) \quad (3.3)$$

where g is degeneracy factor in which the summation runs around a single dirac point. Moreover in the absence of the spin-orbit interactions the form factor is reduced to: $F_{s's}(\vec{k} + \vec{q}, \vec{k}) = \frac{1}{2}[1 + ss' \cos(2\theta)]$, with θ being the angle between k and $k + q$. It should be noted that in this relation the degeneracy factor, g , implies identical contribution of the different Dirac points in the polarization function at given \vec{q} . As discussed before the valley degeneracy could result in identical contribution of the Dirac points in scalar quantities such as total energy. Nevertheless this degeneracy cannot indicate the identical contribution of the Dirac points in the wave number dependent quantities such as polarization function. Consequently, this type of calculations should be performed beyond the Dirac point approximation even when the Fermi energy level lies close to the cones intersecting points. This is due to the fact that the contribution of the different Dirac points, \vec{K}_D and \vec{K}'_D , is not the same and depends on the \vec{K}_D which identifies the position of the Dirac Point in the k -space. This idea has been explained in more details in Appendix: A.

It should be noted that when the integration has been reduced to the Fermi circle of a single Dirac point this assumption automatically ignores the contribution of the inter-valley transitions in which the initial and final states belong to different Fermi circles. This could take place when the transferred momentum, q , satisfies $q \sim |\vec{K}_D - \vec{K}'_D|$. This means that the general form of the Dirac point approximation ignores the inter-valley transition. The anisotropy of the dielectric function results from this type of transitions when the Fermi energy is exactly zero.

The polarization function could be separated into the inter-band (if $s \neq s'$) and the intra-band (if $s=s'$) contributions⁴⁷. Each of these contributions could be classified as intra-band and inter-valley contributions that correspond to different transitions in which the transferred momentum, \vec{q} , is $q \leq k_F < |\mathbf{K}_D - \mathbf{K}'_D|$ or $q \sim |\mathbf{K}_D - \mathbf{K}'_D|$ respectively (where k_F is the radius of the Fermi circle and $\mathbf{K}_D, \mathbf{K}'_D$ are different Dirac points). By means of equation 3.2, we first numerically calculated the polarization function of the graphene, silicene and germanene next using this polarization function the dielectric function (Equation 3.1) has been obtained. We present the result for the $t_{extR} = 0, 0.01, 0.05, 0.1 eV$. Ac-

cording to the present results Broadening of the dielectric function $\epsilon(0, q)$ increases by the Rashba coupling.

IV. FRIEDEL OSCILLATION

To illustrate the oscillations of the screening charge density a charged impurity has been considered to be inserted in the honeycomb structure. The static limit of polarization function is of particular importance as it determines the screened potential of a charge impurity. The screening particle density $\delta n(r)$ due to the central impurity Ze is,

$$\delta n(r) = Ze \frac{1}{(2\pi)^2} \int \left[\frac{V(q) \Pi(0, q)}{\epsilon(0, q)} \right] \exp(iq \cdot r) dq. \quad (4.1)$$

We want to remark that the Friedel oscillation curves in the RPA, the Hubbard vertex correction and Singwer-Sjölander are very similar^{49,51,52}. The reason, for example in the Hubbard Model, is that the Hubbard local field factor $G_H(q)$ is appeared in correlations that are deal with two-body or more, however the screening is essentially a one-body property and the correlations are not appear in one-body amplitudes⁴⁹. The Hamiltonian of graphene-like materials has been considered in tight-binding approximation and the numerical calculations have been performed to obtain band eigenvalues and form factors at each transferred momentum. The extrinsic Rashba interaction could be manipulated by an external gate voltage. By changing the extrinsic Rashba coupling strength, polarization function and consequently the dielectric function will be altered.

V. RESULTS AND DISCUSSION

Dielectric function has been determined by density-density correlations in the system. In the present work this correlation function has been obtained within the random phase approximation. Results of the numerical calculations have been summarized in the following figures. According to the numerical results two-dimensional graphene like materials show anisotropic Friedel oscillations beyond the Dirac cone approximation even when the Dirac points located at the Fermi level. In addition results of the present study show that the extrinsic Rashba coupling has not any considerable effect on the Friedel oscillations. The effect of the spin-orbit couplings is more evident in the Friedel oscillations of the monolayer silicene and germanene. In the presence of the strong intrinsic SOC couplings in these structures the symmetry of the Friedel oscillations in x and y directions has also been removed in an evident manner.

It is important to consider that the general integral expression for the polarization function (Eq. 3.2) goes beyond the states in which the Dirac point approximation is not valid. Nevertheless it should be noted that

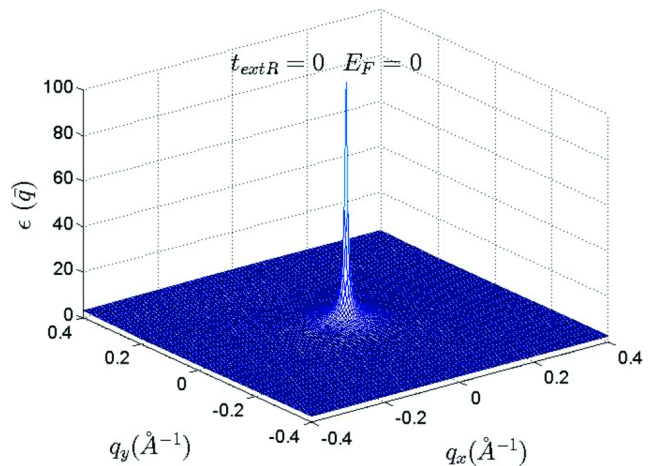


FIG. 3: (Color online) k -space dielectric function of monolayer graphene at $t_{extR} = 0$. Additionally it was assumed that the intrinsic spin-orbit coupling has been also negligible. This enables us to compute the net band induced anisotropic effects.

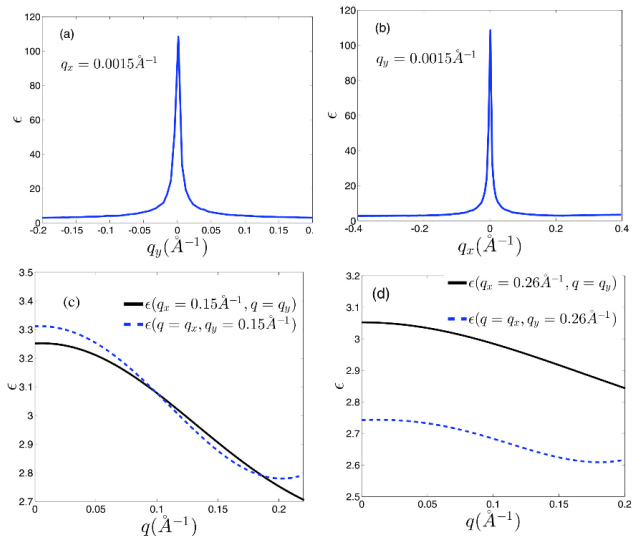


FIG. 4: (Color online) Dielectric function of monolayer graphene at different symmetrically chosen slices for $t_{extR} = 0$ in k -space. (a) At $q_x = 0.0015 \text{ \AA}^{-1}$ plane. (b) $q_y = 0.0015 \text{ \AA}^{-1}$ plane. (c) At $q_x = 0.15 \text{ \AA}^{-1}$ and $q_y = 0.15 \text{ \AA}^{-1}$ slices. (d) At $q_x = 0.26 \text{ \AA}^{-1}$ and $q_y = 0.26 \text{ \AA}^{-1}$ planes. Anisotropic effects appear far away from the origin where the contribution of the inter-valley transitions should be taken into account.

far from the Dirac points most of the states in each band are empty with no contribution in the dielectric function in the static limit ($\hbar\omega = 0$) even at room temperature. For gap-less structures, at room temperature, thermal transitions could be taken place within the range of thermal energy $K_B T = 0.025 \text{ eV}$. Therefore, when the Fermi level is located at the Dirac point the contribution of the

states which were not in the permitted range of the Dirac point approximation automatically have been eliminated by the distribution function implemented in Eq. (3.2). The linear dispersion relation (and therefore circle like Fermi curves) around the Dirac points valid even up to $E_F \sim 1$ eV and the thermal transitions at room temperature with $K_B T = 0.025$ eV could not induce any considerable contribution from those states which have been located far from the Dirac points. So it seems that the Dirac point approximation could still describe the physics of the honeycomb lattice and the linear dispersion relation around the Dirac points could be employed for the calculation of the dielectric function. This means that the non-linear part of the band structure and the anisotropy that might be induced by this part could be ignored. This is due to the fact that this part of the band structure (which could be considered the energy states with $E_k^s > 1$ eV) has not been occupied even as a result of the thermal transitions or could not contribute in the isoenergy transitions of the static limit. However, in the current work we have shown that the contribution of the Dirac points in wave-number dependent quantities should be calculated with some care even when the Dirac point approximation is valid.

When the Fermi energy is close to the Dirac points, each Dirac point has the same contribution in the scalar quantities. Within the Dirac point approximation these contributions are identical for the scalar quantities. Therefore, one could algebraically add up these equivalent contributions to evaluate the amount of the scalar quantity. In this case the contribution of a single Dirac point times the degeneracy factor gives all of the contributions come from the Dirac points as indicated in Eq. (3.3). At low Fermi energies we have the same results even when the Dirac point approximation has not been used. Since the integration of Eq. (3.2) is over the whole Brillouin zone just picks up the significant contributions which mainly are from the states around the Dirac points. Meanwhile it should be noted that for wave number dependent quantities the contribution of each of the Dirac points is not identical at low Fermi energies and even for the zero Fermi energy, $E_F = 0$, the anisotropic contributions come from the inter-valley transitions which can be taken into account when the integration has been performed over the whole Brillouin zone (and not just around a single Dirac point).

There are several studies which have been performed in this field, aiming at an accurate quantitative prediction of dynamical dielectric function, screened charged impurity potential and Friedel oscillations in graphene-like materials. It was realized that the long-distance decay of Friedel oscillations in graphene depends on the symmetry of the scatterer⁵³. In addition a faster, $\delta n \sim 1/r^3$, decay in comparison with conventional 2D electron systems has been observed in Friedel oscillations of a localized impurity inside the monolayer graphene within the Dirac point approximation^{29,53}. However, $1/r$ decay has been reported for bilayer graphene⁵⁴ and strong

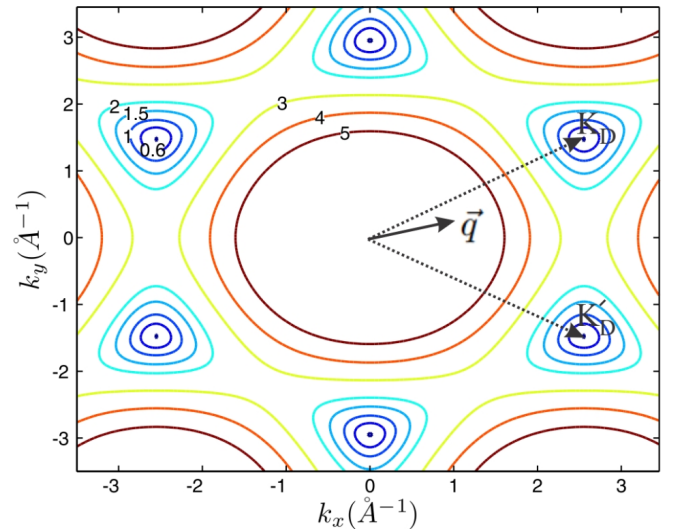


FIG. 5: (Color online) Dirac points of monolayer graphene and Fermi curves at different Fermi energies. Fermi contours have been depicted for $E_F = 0.6$ eV, 1.0 eV, 1.5 eV, 2.0 eV, 3.0 eV, 4.0 eV and 5.0 eV. For a given wave vector \vec{q} the contribution of the different Dirac points on $\epsilon(\vec{q})$ strictly depends on the orientation and position of the \vec{q} with respect to the six Dirac vectors. Trigonal warping of the Fermi curves at different Fermi energies has also indicated in this figure. Single Dirac cone approximation could take into account the anisotropic effects comes from the trigonal warping of a single Fermi curve, however, since the orientation of the deformed Fermi curves are not the same, the anisotropic contribution of the other cones are not identical.

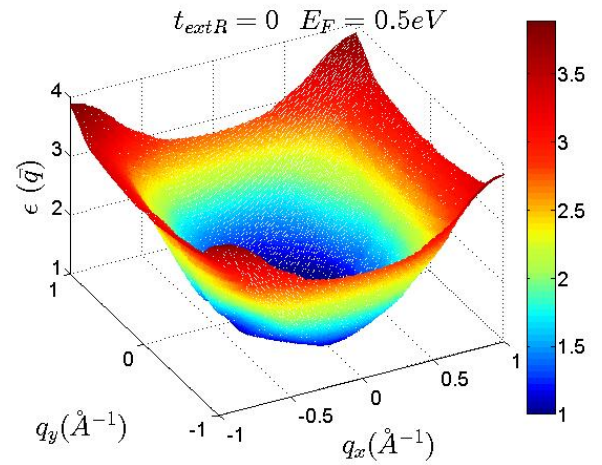


FIG. 6: (Color online) Dielectric function of monolayer graphene for $E_F = 0.5$ eV and $t_{extR} = 0$.

asymmetry and an inverse square-root decay has also been obtained for an anisotropic graphene-like structure when one of the nearest-neighbor hopping amplitudes is different from the others⁵⁵. Recently in rhombohedral graphene multi-layers, $1/r$ decay has been observed for impurity induced Friedel oscillations⁵⁶. Completely

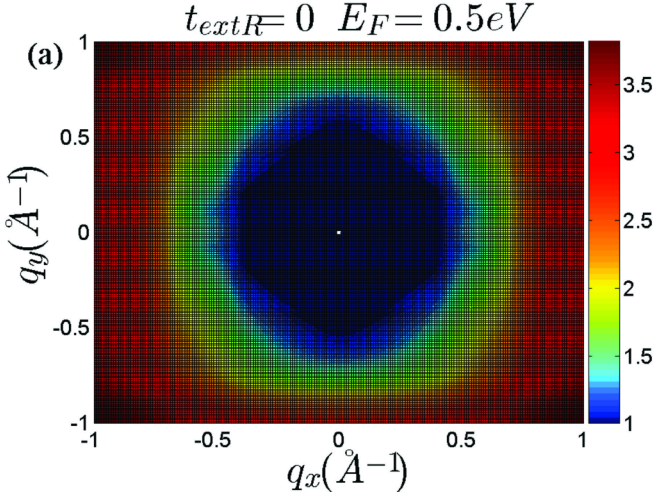


FIG. 7: (Color online) Top view of the dielectric function of monolayer graphene for $E_F = 0.5\text{eV}$ and $t_{\text{ext}R} = 0$. In this case both of the intra-valley and inter-valley transitions result in anisotropic dielectric function in q -space. A hexagon shape contour has been obtained in the inner part of the figure. This hexagon represents the contribution of the intra-valley transitions in the dielectric function of the system which reflects the symmetry bands structure.

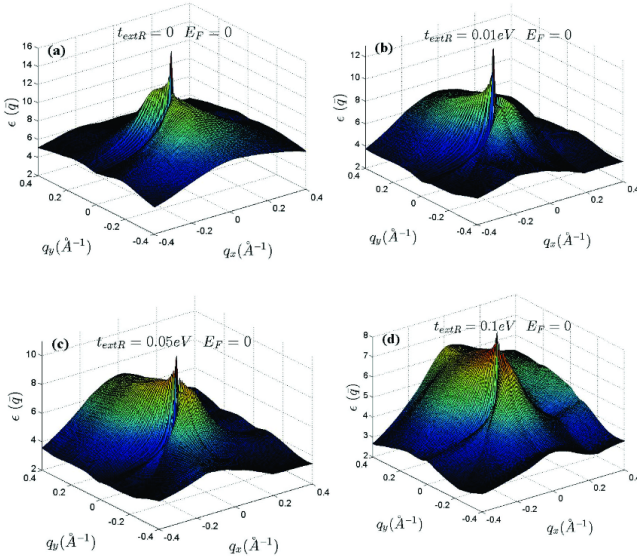


FIG. 8: (Color online) Dielectric function of the monolayer silicene at different Rashba couplings and in the presence of the intrinsic SOC's.

isotropic behavior has been reported for the potential of a screened charged impurity, Friedel oscillations^{28–31} and static dielectric function⁴⁶ within the Dirac point approximation in graphene. Similarly the Dirac point approximation results in isotropic screened potential of a charged impurity in other graphene-like materials such as silicene and germanene²⁶.

It should be noted that the Dirac point approximation

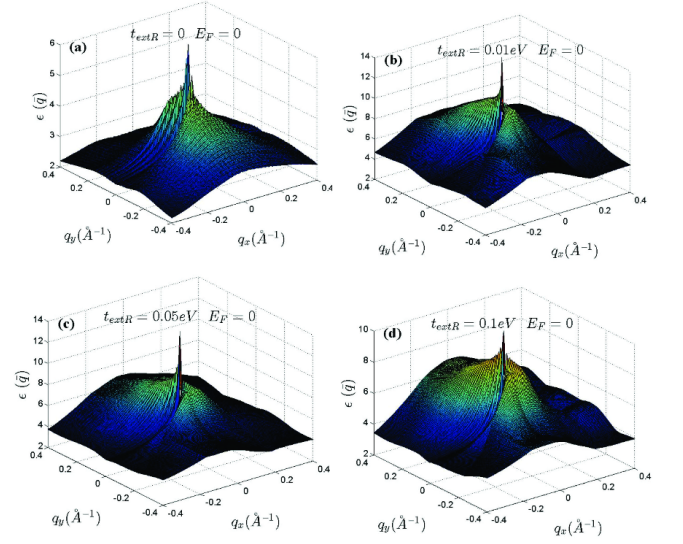


FIG. 9: (Color online) Dielectric function of the monolayer germanene at different Rashba couplings and in the presence of the intrinsic SOC's.

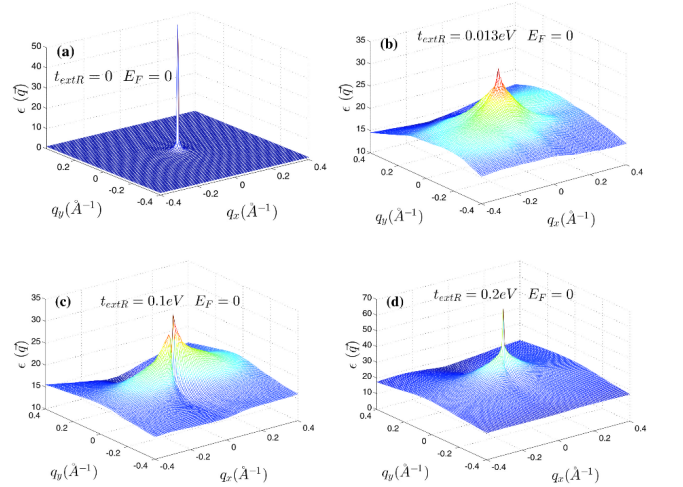


FIG. 10: (Color online) Dielectric function of the bilayer graphene at different Rashba couplings.

based studies give the correct physics of the high wave length limit ($q \ll k_F$) at $E_F = 0$ where inter-valley transitions could not contribute in the physical process. In the absence of the spin-orbit couplings by using the massless linear Dirac spectrum it was also shown that short wavelength spatial dependence of the local density of states leads to anisotropic Friedel oscillations which has the form⁵⁷

$$\delta n(r) \sim c(\vec{r})\rho_0(E_F) \frac{\sin(2k_F r)}{r^2}. \quad (5.1)$$

In which $c(\vec{r})$ is the short wavelength spatial dependence factor and $\rho_0(E)$ is the density of states. Anisotropic dependence of the Friedel oscillations has been introduced

by $c(\vec{r})$ factor which was found to be invariant under threefold rotations⁵⁷. However, if the impurity could not produce inter-valley scatterings this factor is reduced to a constant number⁵⁷. Therefore the anisotropic effects have been removed in the absence of inter-valley transitions⁵⁷. In the current study we have observed that for finite Fermi energies $0 < E_F \leq 1\text{eV}$ even intra-valley transitions are the source of the anisotropic behaviors for linear energy dispersion.

Interestingly it was shown that the Friedel oscillations in graphene have a strong sublattice asymmetry⁵⁸. These calculations have been performed beyond the Dirac point approximation within the Born approximation which can be employed for weak scattering potentials and the stationary phase approximation (SPA) has also been applied for Brillouin zone integrations⁵⁸. Anisotropic Friedel oscillations could also be inferred from the numerical results of the recent work in the absence of the spin-orbit interactions especially over short distances.

It seems that the degeneracy of the K-points results in identical contribution of each Dirac point in all of the physical quantities when the Fermi energy is close to the Dirac points. However, it should be noted that, this is not the case for some of the quantities which directly depending on the direction of the transferred wave number. In this case due to the anisotropic position of the Dirac points in the Brillouin zone each of the Dirac points has not identical contribution for this type of the quantities even when the Dirac point approximation is valid.

Anisotropic Friedel oscillations in two-Dimensional structures have been observed before⁵⁹. However, in the present case the anisotropic effects are direct manifestation of non-identical contribution of Fermi circles and Dirac points in wave number dependent quantities. Some of the physical quantities, such as dielectric function, are given by integration over the Brillouin zone as expressed in Eq. (3.2). This integration goes beyond the states in which the Dirac point approximation and the linear dispersion relation no longer valid. However distribution function at low temperatures and Fermi energies picks up the contribution of the states which were located near to the Dirac points. Nevertheless for evaluating non-scalar quantities that depending on the wave number and its direction we should consider that the orientation of the wave number, q , (relative to the position vector of the Dirac points in k-space) determines the contribution of each Dirac point. It can be clearly demonstrated that the dielectric function shows anisotropic directional in q -space (See Appendix: A).

It should be noted that increasing of the Fermi energy results in deformation of circle-like Fermi curves (Fermi-circles) of low Fermi energies around the Dirac points. In this case the isotropic form of the Fermi circles change into the trigonal-shaped contours (known as trigonal warping effect) and the isotropic form of the Fermi curve around of the Dirac points has totally been removed at high Fermi energies. This type of deformation could results in a new source of anisotropy at high Fermi

energies which has not considered in the current work which was limited to the low Fermi energies.

Due to the foregoing discussion for wave number-dependent or non-scalar quantities such as dielectric function, electric and thermal conductivities we have to concern about the position of the Dirac points relative to the direction of the characteristic vector of the physical quantity (such as transferred momentum) even when the Dirac point approximation is valid. For sharp scattering potentials we have to consider the inter-valley transitions in this type of the quantities. Within the Dirac point approximation the integration over the state-resolved contributions is generally performed over a single Fermi circle. This could be a correct approach when we assume the identical contribution of each Dirac point and ignore the inter-valley transitions. In this case if we put aside the Dirac point approximation and perform the integration over the whole Brillouin zone the correct contribution of each Dirac point could be obtained. This means that beyond the Dirac point approximation dielectric function and therefore Friedel oscillations for graphene-like honeycomb structures should be anisotropic in k -space and the real space respectively.

At low Fermi energies optical transitions around each Dirac points, where take place within a single Fermi circle, have the main contribution in the dielectric function of the honeycomb systems. This manifests itself as a central peak of the dielectric function in the middle of the Brillouin zone. It could be shown that beyond the Dirac point approximation the central peak contains the contribution of all of the Dirac points.

When the Fermi energy is close to Dirac points ($E_F = 0$) and at the high wave length limit ($q \ll |K_D - K'_D|$) the occupation factor $f_k^s - f_{k'}^{s'}$ could have a significant value only when the k and k' states are close to a single Dirac point of different bands ($s \neq s'$). Meanwhile $\delta_{\vec{k}', \vec{k} + \vec{q}}$ in the expression of the polarization indicates that the contribution of the Dirac points should be selected by Γ -point ($\vec{q} = 0$). Since at this limit the main contribution is due to the intra-valley transitions which take place near the Dirac points in which $k \approx K_D$ and $k' \approx K_D$ therefore the mentioned Dirac delta function, which reflects the momentum conservation, imposes that the contribution of the Dirac points should be manifest themselves at the Γ -point ($\vec{q} \approx 0$) of the q -space.

The mentioned argument reveals the fact that the central peak of the dielectric function is exactly sum of all of the contributions from each Dirac point. In this step since the main contribution belongs to the case of zero transferred momentum ($q \sim 0$) the question of the anisotropy in q -space is quite irrelevant at $E_F = 0$ (see Appendix: A). However, it should be noted that the contribution of inter-valley transitions between different Dirac points ($q \sim |K_D - K'_D|$) are not identical. In this case the contribution of each pair of contributing Dirac point (\mathbf{K}_D and \mathbf{K}'_D) has been determined by the direction of the \vec{q} vector (Appendix: A).

In order to obtain the anisotropic effects which have

been induced merely by band energy we have to switch off both types of the spin orbit couplings. It was reported that the Rashba coupling strength in graphene is greater than the intrinsic spin orbit interaction. we have ignored intrinsic spin orbit coupling in monolayer and bilayer graphene. At zero Rashba interaction both intrinsic and extrinsic spin-orbit couplings are absent. This enables us to obtain the anisotropic effects which could be induced merely by band energy. Dielectric function at zero Rashba coupling and zero Fermi energy ($E_F = 0$) has been obtained as depicted in Fig. (3). At the first look it seems that there is no anisotropy, however, it should be noted that the anisotropy of the dielectric function has been hidden behind the large central peak at $q \sim 0$. Since the amount of the dielectric anisotropy is very small in comparison with the value of the dielectric function at the Γ -point. This fact prevents the identification of the directional dependence of the dielectric function. At low wave numbers i.e. in the range of the intra-valley transitions dielectric function seems to be quite isotropic in q -space Fig. (4 (a) and (b)). However, far from the central region if we select different symmetric slices of the dielectric surface, the anisotropy of the dielectric function will be evident Fig. (4 (c) and (d)). This figure shows that for different directions of the k -space behavior of the dielectric function are quite different. This means that the contributing inter-valley transitions in finite wave length limit ($q \sim |K_D - K'_D|$) introduces the anisotropic behaviors.

When the Dirac points are not located exactly on the Fermi level the intra-valley transitions could take place within the range of $q \leq k_F$. Meanwhile we have assumed that the Fermi energy is still low enough to employ the linear dispersion relation of the Dirac cone. It can be shown that both of the intra-valley ($q \leq k_F$ for this case) and inter-valley transitions should be considered as anisotropic contributions in the dielectric function (Figs. 6 and 7). In this case since the inter-band transitions ($|k\lambda_k^s \rightarrow k'\lambda_{k'}^{s'}|$, $s \neq s'$) are absent in the static limit ($\hbar\omega = 0$) therefore all of the contributing terms (both intra-valley and inter-valley transitions) are intra-band. Consequently, $q = 0$ transitions could not contribute in the static dielectric function. Since it can be shown that for $E_F \neq 0$ we have $F_{ss'}(\vec{k} + \vec{q}, \vec{k}) = 0$ when $q = 0$ and $s \neq s'$. As shown in Figs. 6 and 7 at low transferred momentums since at this limit of the wave vectors just the intra-valley transitions could contribute in the dielectric function of the honeycomb structure. So the band anisotropy reflects itself in the anisotropy of the dielectric function with a sixfold symmetry at the range of short wave numbers (Fig. 7). This symmetric shape has been modified at high wave numbers where the inter-valley transitions start to contribute in the static dielectric function Fig. 7).

As shown in Figs. (8)-(10) dielectric function will be broadened in the presence of the Rashba coupling in graphene-like structures. Moreover the central peak of the dielectric function in silicene and germanene will also

be broadened in the presence of the intrinsic spin-orbit coupling. Increasing the Rashba interaction increases the broadening of the dielectric function at the central region. Since the Rashba interaction removes the inversion symmetry in the system. This symmetry breaking leads to anti-symmetric dielectric function in the presence of the Rashba interaction and it could be recognized that $\epsilon(\vec{q}) \neq \epsilon(-\vec{q})$.

The anisotropy of the dielectric function as discussed before is due to the non-identical contribution of the Dirac points and the nonlinear part of the spectrum cannot contribute in dielectric function when the Fermi level is close to the Dirac points. Increasing the Rashba coupling strength slightly modifies the dielectric function in silicene and germanene however the change of the dielectric function of the monolayer and bilayer graphene is relatively significant. As a result, it is expected that the influence of the Rashba interaction in the Friedel oscillations of the monolayer and bilayer graphene is more pronounced as compared to that of other selected honeycomb structures where Figs. (11)-(14) exactly indicates this fact. This could be explained if we consider relatively large and dominant intrinsic spin-orbit coupling in silicene and germanene. As shown in the figures

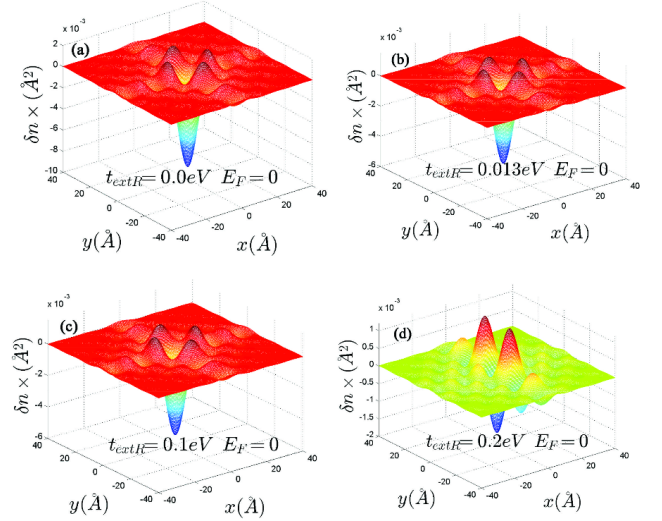


FIG. 11: (Color online) Real space anisotropic Friedel oscillations in monolayer graphene at different Rashba couplings.

(11)-(14) the anisotropic Friedel oscillations have been observed even when the Rashba coupling strength is very low or zero. It can be inferred from the results of the current work that the Rashba coupling is less effective in the generation of the anisotropy. Therefore one can conclude that the anisotropy of the dielectric function and Friedel oscillations mainly depends on the anisotropy of the band structure in k -space.

As shown in Fig. (5) band induced anisotropic effects have been reflected in the Friedel oscillations of the graphene-like structures. As depicted in Fig. (5) at low Fermi energies the Fermi curves have been appeared as

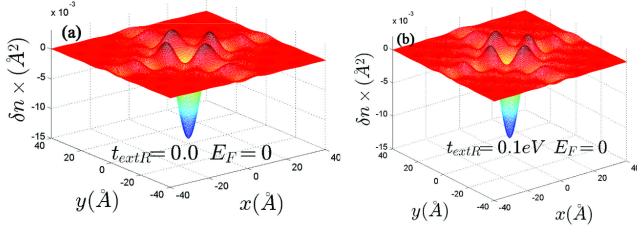


FIG. 12: (Color online) Real space anisotropic Friedel oscillations in monolayer silicene at different Rashba couplings.

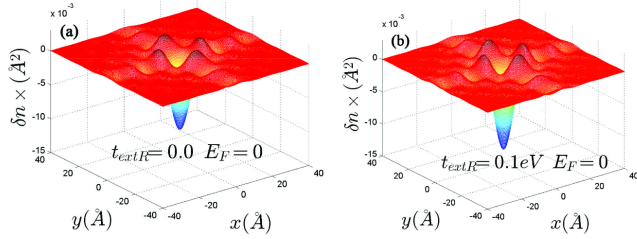


FIG. 13: (Color online) Real space anisotropic Friedel oscillations in monolayer germanene at different Rashba couplings.

separated islands around each Dirac point. Therefore the amount of the dielectric and polarization functions in a given \vec{q} wave number have significantly been determined by the orientation of the wave number with respect to the Dirac points position vectors. This anisotropy of the q -space has been reflected in the real space quantities such as Friedel oscillations as depicted in Figs. (11)–(14).

When Dirac point approximation is valid, Fermi level is appeared as distinct circular curves in k -space known as Fermi circles. One might conclude that the circular shape of the Fermi contour around of the Dirac points implies that all of the extractable physical properties of the system should be isotropic as long as the Dirac point approximation is application. However it should be considered that the isotropic and circular shape of the Fermi contours around of the Dirac points cannot indicate isotropic properties in all of the conditions. This is due to the fact that the Dirac points themselves are located in k -space in anisotropic way. On the other hand even if the contribution of the states around a given Dirac point is isotropic and even if the contribution of the Dirac points are identical the location of the Dirac points in the Brillouin zone is still anisotropic. The degeneracy of the Dirac points results in identical contribution of these points in the scalar quantities of the system. However, in calculation of vector and tensor dependent quantities we should consider that the contribution of inter-valley transitions cannot be identical in all of the q -space directions even when $E_F = 0$. Moreover when $E_F > 0$ both of the intra-valley and inter-valley transitions result in anisotropic dependence of the dielectric function in q -space. Therefore different directions in the q -space have not identical con-

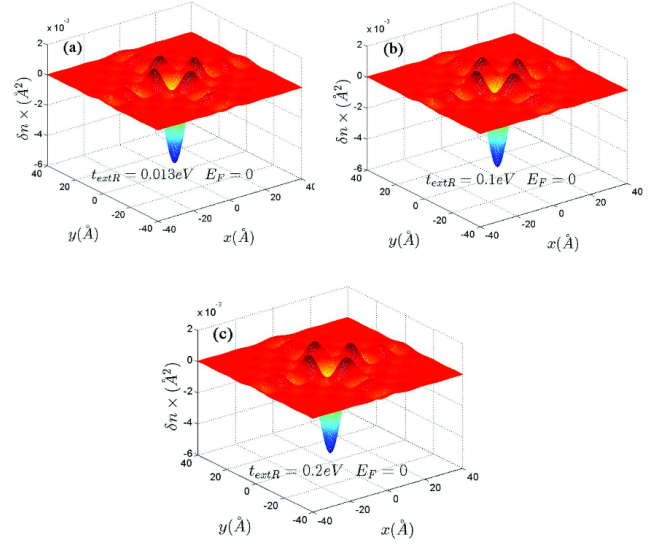


FIG. 14: (Color online) Real space anisotropic Friedel oscillations in bilayer graphene at different Rashba couplings.

tribution even when the Dirac points are identical and degenerate. Accordingly the conventional Dirac point approximation could not describe all of the physics of the vector or vector dependent parameters at low wavelength limit. This could also result in anisotropic electric and thermal conductivity in graphene-like materials for short range scatterers (for example in the case of the delta-shaped scatterers) in which all of the intra-valley and inter-valley scatterings are possible.

Finally it is important to note, the anisotropy of the dielectric function suggests that the orientation of the bases vectors of the honeycomb lattice could be determined by full optical measurements. Since dynamical dielectric function of the graphene-like materials are possibly have the same anisotropic nature. Therefore the absorption spectra of the system should be anisotropic. Accordingly, the real space orientation of the basis vectors could be explored since the absorption spectra leads to identification of the band energy configuration in k -space.

VI. CONCLUSION

In conclusion, we have analyzed the band induced anisotropic effects in graphene-like structures. We have also investigated the influence of the spin-orbit interactions on dielectric function and Friedel oscillations in this type of materials. Based on RPA formalism, which accounts for electron-electron scattering, we have shown that the Dirac points have not identical contribution for wave number dependent quantities such as dielectric function even when the Fermi energy is close to these points. The main limitations for the use of the Dirac point approximation has been discussed within the

current work. Non-identical contribution of the Dirac points results in anisotropic dielectric function in k -space. Moreover, the anisotropic function leads to anisotropic Friedel oscillation in graphene-like materials.

The influence of the Rashba SOC on the dielectric function and Friedel oscillations has also been discussed in the present study where we have shown that increasing the Rashba coupling strength slightly modifies the dielectric function. Meanwhile in the presence of the Rashba interaction the inversion symmetry of the dielectric function has been lifted in k -space.

Appendix: A

Different types of transitions could be contributed in the dielectric function of the honeycomb structures. In this case transitions could be either intra-valley or inter-valley. Where in the intra-valley transitions initial and final states \vec{k} and \vec{k}' belong to the same Dirac valley cone while in the inter-valley transitions \vec{k} and \vec{k}' belong to different Dirac cones (Fig. 15 (a) and (b)). The momentum conservation rule for each transition between the states \vec{k} and \vec{k}' with transferred momentum \vec{q} could be satisfied when \vec{k} and \vec{k}' sweep the Fermi circles as shown in Fig. 15. It can be inferred that this condition could be satisfied for intra-valley transitions when $0 \leq q \leq k_F$ where k_F is the radius of the Fermi circle Fig. 15 (a) and inter-valley transitions could take place $q \sim |\mathbf{K}_D - \mathbf{K}'_D|$ where \mathbf{K}_D and \mathbf{K}'_D are different Dirac points.

Fig. 15 shows the Fermi circles of a planar honeycomb lattice has been depicted in the absence of the SOC. It can be shown that due to this six-fold band rotational symmetry of the system if the transition rule is satisfied for a given transferred momentum (\vec{q}) it will also be satisfied for the sixfold rotated wave number $\mathcal{R}_{2\pi/6}^n \vec{q}$ (Fig. 15 (a) and (b)). In which $\mathcal{R}_{2\pi/6}$ is the sixfold rotation operator. This means that

$$\begin{aligned} \delta_{\vec{k}+\vec{q},\vec{k}'} &= \delta_{\mathcal{R}_{2\pi/6}^n \vec{k} + \mathcal{R}_{2\pi/6}^n \vec{q}, \mathcal{R}_{2\pi/6}^n \vec{k}'} \\ &= \delta_{\vec{k}_n + \vec{q}_n, \vec{k}'_n} \end{aligned} \quad (\text{A.1})$$

Meanwhile the form factor of the graphene is also invariant under the sixfold rotations in the absence of the spin-orbit couplings.

$$F_{s's}(\vec{k} + \vec{q}, \vec{k}) = F_{s's}(\mathcal{R}_{2\pi/6}^n \vec{k} + \mathcal{R}_{2\pi/6}^n \vec{q}, \mathcal{R}_{2\pi/6}^n \vec{k}) \quad (\text{A.2})$$

In both cases i.e. for inter-valley and intra-valley transitions band symmetry of the honeycomb structures manifests itself as $E_{\vec{k}}^s = E_{\mathcal{R}_{2\pi/6}^n \vec{k}}^s$. Therefore Eq. 3.2 reveals that for a given transferred momentum, \vec{q} , satisfying the transition rule $\vec{k} = \vec{k}' - \vec{q}$. The contribution of the \vec{k} -state in the dielectric function is identical with the contributions of the rotated states: $\mathcal{R}_{2\pi/6} \vec{k}$, $\mathcal{R}_{2\pi/6}^2 \vec{k}$, ..., $\mathcal{R}_{2\pi/6}^5 \vec{k}$ regardless of the inter-valley or intra-valley nature of the transitions. In the other words it could be inferred that

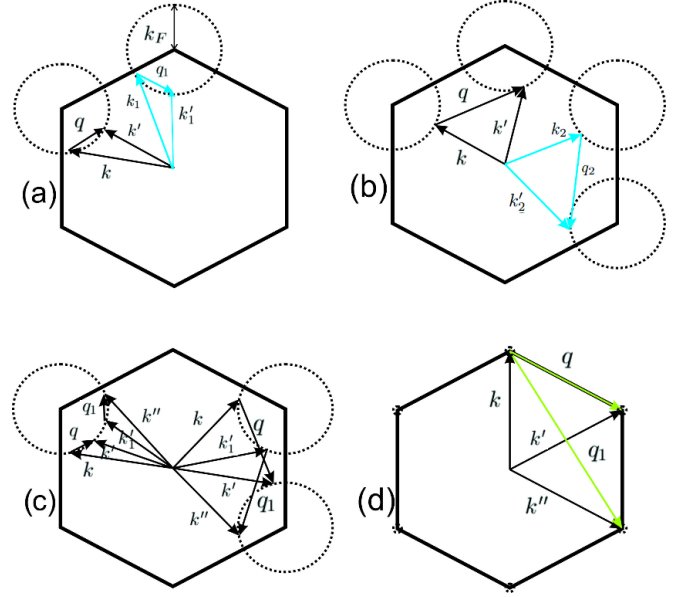


FIG. 15: (Color online) Intra-valley (a) and inter-valley (b) transitions for a given transferred momentum \vec{q} . When the transition rule (or momentum conservation rule) is satisfied for \vec{q} the initial and final states should be placed on the Fermi circles. In this case the contribution of the given states (black vectors) is identical with the contribution of the sixfold-rotated states (cyan vectors). One can imagine about another type of possible transitions (c) with constant value of the transferred momentum $q = q_1$ between the equi-energy states $E_k^s = E_{k'}^s = E_{k_1}^s = E_{k''}^s$, where the corresponding pair vectors ($\vec{q} \vec{q}_1$), ($\vec{k} \vec{k}_1$) and ($\vec{k}' \vec{k}''$) are not related by sixfold symmetry operators e.g. $\mathcal{R}_{2\pi/6}^n \vec{q} \neq \vec{q}_1$. It can be shown that form factor of these transitions are different i.e. $F(k, k') \neq F(k_1, k'')$. At zero Fermi energy (d) i.e. when $k_F = 0$ intra-valley transitions occur at $q = 0$ which result in central peak of the dielectric function. However inter-valley transitions (light green vectors) are still the source of anisotropy of the dielectric function.

$\epsilon(\vec{q}) = \epsilon(\mathcal{R}_{2\pi/6} \vec{q}) = \epsilon(\mathcal{R}_{2\pi/6}^2 \vec{q}) \dots = \epsilon(\mathcal{R}_{2\pi/6}^5 \vec{q})$. For example in the case of intra-valley transitions the different Dirac point or Fermi curves which have been related by sixfold rotation operators have the same contribution in the dielectric function for those transferred momentums which have the same symmetry relation. Consequently, the contribution of the Fermi circle located around the (\vec{K}_D Dirac point on the dielectric function of \vec{q} is identical with the contribution of ($\vec{K}_D^{(i)}$ Fermi circle on the dielectric function of $\mathcal{R}_{2\pi/6}^i \vec{q}$ when these two Dirac points are related by $\vec{K}_D^{(i)} = \mathcal{R}_{2\pi/6}^i \vec{K}_D$. If we continue the same procedure for parallel wave numbers, which satisfying the transition rule, one can realize the anisotropy of the dielectric function which manifests itself by sixfold symmetric curve at low transferred momentums Fig. 7. These relations identify different class of the states which have identical contribution in the dielectric function i.e. the for different states with transferred momentum q in

this case the class of the identical contributions for both inter and intra valley transitions is specified by

$$[q] = \{\vec{q}, \mathcal{R}_{2\pi/6}\vec{q}, \mathcal{R}_{2\pi/6}^2\vec{q}, \dots, \mathcal{R}_{2\pi/6}^5\vec{q}\}. \quad (\text{A.3})$$

Which corresponds to the transitions: $\vec{k} \rightarrow \vec{k} + \vec{q}$, $\mathcal{R}_{2\pi/6}^5\vec{k} \rightarrow \mathcal{R}_{2\pi/6}\vec{k} + \mathcal{R}_{2\pi/6}\vec{q}$, $\dots, \mathcal{R}_{2\pi/6}^5\vec{k} \rightarrow \mathcal{R}_{2\pi/6}\vec{k} + \mathcal{R}_{2\pi/6}\vec{q}$.

The first consequence of the above argument is that the different Fermi curves of each Dirac point have not identical contribution on the dielectric function at a given \vec{q} wave number. In the other words the contribution of each Fermi circle (corresponding to K_D dirac point) with a given transferred momentum, \vec{q} , has been determined by the orientation of the \vec{q} with respect to the K_D . When \vec{q} satisfies the transition rule for a specific Dirac cone (for example in an intra-valley process) this rule will be satisfied for $\mathcal{R}_{2\pi/6}^n\vec{q}$ ($n = 1..5$) at other Dirac cones and \vec{q} itself could not satisfy the momentum conservation rule or could not give the same contribution at these Dirac cones. Therefore the contribution of different Fermi circles on the dielectric function of \vec{q} is not identical. Accordingly the dielectric function should be anisotropic in the q -space with sixfold symmetry which was originated from the symmetry of the band structure.

All of the other possible transitions with a given fixed

value of the transferred momentum could take place between the isoenergy states as shown in Fig. 15 (c). In this group of the transition transferred momentum is the same $q = q_1$ and both of the initial final states are located at Fermi circle $E_k^s = E_{k'}^s = E_{k_1'}^s = E_{k''}^s = E_F$. However, corresponding pair vectors are not related by sixfold symmetry operators i.e. $\mathcal{R}_{2\pi/6}^n\vec{q} \neq \vec{q}_1$, $\mathcal{R}_{2\pi/6}^n\vec{k} \neq \vec{k}_1'$ and $\mathcal{R}_{2\pi/6}^n\vec{k}' \neq \vec{k}''$. The transition rule has been satisfied for these transition where we have $\vec{k} + \vec{q} = \vec{k}'$ and $\vec{k}_1' + \vec{q}_1 = \vec{k}''$. Meanwhile, the form factor of the transitions are not the same $F(k, k') \neq F(k_1', k'')$ which implies that the corresponding contributions are not identical (Fig. 15 (c)).

When the Fermi energy located at Dirac points i.e. $E_F = 0$ then the intra-valley transitions occur in $\vec{q} = 0$ between different bands (Fig 15 (d)). Unlike the previous case the intra-valley contributions are identical here. These contributions result in the central peak of the dielectric function. Since the $V(q) = 2\pi e^2/q$ diverges at $q = 0$ where the intra-valley transitions could contribute at this point. However the inter-valley transitions occur away from the Γ -point ($q = 0$) result in anisotropic contributions as the previous case. Therefore one can expect that the anisotropy of the dielectric function would be appeared at $q \geq |\mathbf{K}_D - \mathbf{K}'_D|$ Fig 4.

* Electronic address: phirouznia@azaruniv.ac.ir

- ¹ K. S. Novoselov, A. K. Geim, S. Morozov, D. Jiang, Y. Zhang, S. Dubonos, I. Grigorieva, and A. Firsov, science **306**, 666 (2004).
- ² A. K. Geim and K. S. Novoselov, Nature materials **6**, 183 (2007).
- ³ Y. Xu, B. Yan, H.-J. Zhang, J. Wang, G. Xu, P. Tang, W. Duan, and S.-C. Zhang, Phys. Rev. Lett. **111**, 136804 (2013).
- ⁴ G. G. Guzmán-Verri and L. L. Y. Voon, Phys. Rev. B **76**, 075131 (2007).
- ⁵ S. Cahangirov, M. Topsakal, E. Aktürk, H. Şahin, and S. Ciraci, Phys. Rev. Lett. **102**, 236804 (2009).
- ⁶ C.-C. Liu, W. Feng, and Y. Yao, Phys. Rev. Lett. **107**, 076802 (2011).
- ⁷ F. Liu, C.-C. Liu, K. Wu, F. Yang, and Y. Yao, Phys. Rev. Lett. **111**, 066804 (2013).
- ⁸ L. Chen, C.-C. Liu, B. Feng, X. He, P. Cheng, Z. Ding, S. Meng, Y. Yao, and K. Wu, Phys. Rev. Lett. **109**, 056804 (2012).
- ⁹ P. Vogt, P. De Padova, C. Quaresima, J. Avila, E. Frantzeskakis, M. C. Asensio, A. Resta, B. Ealet, and G. Le Lay, Phys. Rev. Lett. **108**, 155501 (2012).
- ¹⁰ L. Chen, H. Li, B. Feng, Z. Ding, J. Qiu, P. Cheng, K. Wu, and S. Meng, Phys. Rev. Lett. **110**, 085504 (2013).
- ¹¹ B. Feng, Z. Ding, S. Meng, Y. Yao, X. He, P. Cheng, L. Chen, and K. Wu, Nano letters **12**, 3507 (2012).
- ¹² C.-C. Liu, W. Feng, and Y. Yao, Phys. Rev. Lett. **107**, 076802 (2011).
- ¹³ S. Cahangirov, M. Topsakal, E. Aktürk, H. Şahin, and S. Ciraci, Phys. Rev. Lett. **102**, 236804 (2009).

- ¹⁴ G. G. Guzmán-Verri and L. L. Y. Voon, Phys. Rev. B **76**, 075131 (2007).
- ¹⁵ X. Lin and J. Ni, Phys. Rev. B **86**, 075440 (2012).
- ¹⁶ K. Takeda and K. Shiraishi, Phys. Rev. B **50**, 14916 (1994).
- ¹⁷ E. Durgun, S. Tongay, and S. Ciraci, Phys. Rev. B **72**, 075420 (2005).
- ¹⁸ M. Ezawa, Phys. Rev. B **87**, 155415 (2013).
- ¹⁹ N. Drummond, V. Zolyomi, and V. Fal'Ko, Phys. Rev. B **85**, 075423 (2012).
- ²⁰ M. Ezawa, New Journal of Physics **14**, 033003 (2012).
- ²¹ N. Drummond, V. Zolyomi, and V. Fal'Ko, Phys. Rev. B **85**, 075423 (2012).
- ²² M. Ezawa, Phys. Rev. Lett. **109**, 055502 (2012).
- ²³ Y. Zhang, T.-T. Tang, C. Girit, Z. Hao, M. C. Martin, A. Zettl, M. F. Crommie, Y. R. Shen, and F. Wang, Nature **459**, 820 (2009).
- ²⁴ A. Grigorenko, M. Polini, and K. Novoselov, Nature photonics **6**, 749 (2012).
- ²⁵ F. Bonaccorso, Z. Sun, T. Hasan, and A. Ferrari, Nature Photonics **4**, 611 (2010).
- ²⁶ C. J. Tabert and E. J. Nicol, Phys. Rev. B **89**, 195410 (2014).
- ²⁷ R. Roldán and L. Brey, Phys. Rev. B **88**, 115420 (2013).
- ²⁸ A. Scholz, T. Stauber, and J. Schliemann, Phys. Rev. B **86**, 195424 (2012).
- ²⁹ B. Wunsch, T. Stauber, F. Sols, and F. Guinea, New Journal of Physics **8**, 318 (2006).
- ³⁰ G. Gómez-Santos and T. Stauber, Phys. Rev. Lett. **106**, 045504 (2011).
- ³¹ V. V. Cheianov and V. I. Fal'ko, Phys. Rev. Lett. **97**, 226801 (2006).

- ³² M. J. Schmidt, M. Golor, T. C. Lang, and S. Wessel, Phys. Rev. B **87**, 245431 (2013).
- ³³ C.-C. Liu, H. Jiang, and Y. Yao, Phys. Rev. B **84**, 195430 (2011).
- ³⁴ H. Min, J. E. Hill, N. A. Sinitsyn, B. R. Sahu, L. Kleinman, and A. H. MacDonald, Phys. Rev. B **74**, 165310 (2006).
- ³⁵ Y. A. Bychkov and E. I. Rashba, Journal of physics C: Solid state physics **17**, 6039 (1984).
- ³⁶ A. C. Neto, F. Guinea, N. Peres, K. S. Novoselov, and A. K. Geim, Rev. Mod. Phys. **81**, 109 (2009).
- ³⁷ V. N. Kotov, B. Uchoa, V. M. Pereira, F. Guinea, and A. C. Neto, Rev. Mod. Phys. **84**, 1067 (2012).
- ³⁸ R. van Gelderen and C. M. Smith, Phys. Rev. B **81**, 125435 (2010).
- ³⁹ Z. Qiao, X. Li, W.-K. Tse, H. Jiang, Y. Yao, and Q. Niu, Phys. Rev. B **87**, 125405 (2013).
- ⁴⁰ T. Ando, A. B. Fowler, and F. Stern, Rev. Mod. Phys. **54**, 437 (1982).
- ⁴¹ G. Giuliani and G. Vignale, *Quantum theory of the electron liquid* (Cambridge university press, 2005).
- ⁴² K. Kaasbjerg, K. S. Thygesen, and A.-P. Jauho, Phys. Rev. B **87**, 235312 (2013).
- ⁴³ P. Pyatkovskiy, J. Phys.: Conf. Ser. **129**, 012006 (2008).
- ⁴⁴ P. Pyatkovskiy, Journal of Physics: Condensed Matter **21**, 025506 (2009).
- ⁴⁵ E. Gorbar, V. Gusynin, V. Miransky, and I. Shovkovy, Phys. Rev. B **66**, 045108 (2002).
- ⁴⁶ E. Hwang and S. D. Sarma, Phys. Rev. B **75**, 205418 (2007).
- ⁴⁷ R. Sensarma, E. Hwang, and S. D. Sarma, Phys. Rev. B **82**, 195428 (2010).
- ⁴⁸ A. Scholz, T. Stauber, and J. Schliemann, Phys. Rev. B **88**, 035135 (2013).
- ⁴⁹ G. D. Mahan, *Many-particle physics* (Springer, 2000).
- ⁵⁰ C. Hwang, D. A. Siegel, S.-K. Mo, W. Regan, A. Ismach, Y. Zhang, A. Zettl, and A. Lanzara, Scientific Reports **2**, 590 (2012).
- ⁵¹ J. Hubbard, Proceedings of the Royal Society of London. Series A. Mathematical and Physical Sciences **243**, 336 (1958).
- ⁵² K. Singwi, A. Sjölander, M. Tosi, and R. Land, Phys. Rev. B **1**, 1044 (1970).
- ⁵³ V. V. Cheianov, The European Physical Journal Special Topics **148**, 55 (2007).
- ⁵⁴ C. Bena, Phys. Rev. Lett. **100**, 076601 (2008).
- ⁵⁵ C. Dutreix, L. Bileanu, A. Jagannathan, and C. Bena, Phys. Rev. B **87**, 245413 (2013).
- ⁵⁶ C. Dutreix and M. I. Katsnelson, Phys. Rev. B **93**, 035413 (2016).
- ⁵⁷ A. Bácsi and A. Virosztek, Phys. Rev. B **82**, 193405 (2010).
- ⁵⁸ J. A. Lawlor, S. R. Power, and M. S. Ferreira, Physical Review B **88**, 205416 (2013).
- ⁵⁹ P. Hofmann, B. Briner, M. Doering, H.-P. Rust, E. Plummer, and A. Bradshaw, Phys. Rev. Lett. **79**, 265 (1997).